RSC Advances

PAPER

Drying of particle-loaded foams for production of porous materials: mechanism and theoretical modeling†

Cite this: *RSC Adv.*, 2014, **4**, 811

I. Lesov, S. Tcholakova* and N. Denkov

Particle-loaded wet foams are appropriate precursors for production of novel porous materials with hierarchical porous structure, ranging from tens of micrometers down to a few nanometers. Such porous materials could be further modified (sintered, impregnated, hydrophobized, *etc.*) to serve as catalyst supports, porous filters, insulating materials, templates for composite materials, *etc.* A particular obstacle for the design of such materials is the observed extensive shrinkage during drying of the wet foam precursor. This shrinkage has three important consequences – significant reduction of the size of the final porous material (as compared to the precursor template), significant evolution in the pore size distribution during sample drying, and possible cracking of the material upon drying. The major aims of the current study are (1) to clarify the main mechanism of shrinkage of foams prepared from silica suspensions with high particle concentration, and (2) to describe quantitatively the relation between the properties of the foamed suspension and the final dry porous material obtained from this suspension. The performed experiments and the data interpretation convincingly show that the foamed suspensions shrink until the particle concentration in the foam walls reaches close packing, at which the percolated particle structure is able to resist the high capillary pressures, developed in the process of drying. The volumetric shrinkage of the individual bubbles was found to be equal to that of the macroscopic foam sample. Equations are derived and verified to relate the particle concentration and the bubble fraction in the foam precursor with the final mass density of the obtained porous material and with the degree of shrinkage in the drying process. Three stages of foam drying and shrinking were observed: (1) an induction period with no sample shrinkage, despite the water loss, (2) rapid shrinkage, and (3) final water evaporation at constant volume of the sample. These stages were explained by considering the three basic physical regimes of convective drying of porous materials, as defined by Coussot (European Phys. J. B 15 (2000) 557–566). The equations derived in the current study allow one to design in advance the foam precursors needed to obtain a dry porous material with desired properties.

Received 20th August 2013
Accepted 28th October 2013

DOI: 10.1039/c3ra44500c

www.rsc.org/advances

1. Introduction

Porous ceramics are a unique class of materials with low mass density and high surface area that make them desirable for various applications, ranging from insulating construction panels to highly effective catalyst supports or templates for tissue scaffolds. Due to these versatile applications, a vast number of papers on the methods for production and on the properties of porous ceramic materials have been published in the last decade. Reviews on the typical pathways for their preparation can be found in Binner,[1] Colombo,[2] and Gonzenbach *et al.*[3]

One of the simplest methods for preparation of very light porous ceramic materials is the direct foaming method.[4] It consists of mechanical agitation of particle suspension in the presence of appropriate surfactant, with subsequent removal of the water from the obtained wet aerated (foam) precursor. Water could be either evaporated or physically/chemically bound through a series of complex procedures.[3] One important feature of these systems is that one can use appropriate combinations of nano-structured particles (*e.g.* fractal silica) with micrometer-sized bubbles to design ceramic materials with complex pore size distributions.[5] However, to apply intelligently this procedure, one should understand the processes of material shrinkage and pore-size evolution during drying of the wet precursors.

The process of water evaporation from porous media such as sols, gels and foods has been widely discussed in the literature[6–22] in the more general context of producing dry final products from wet precursors. Typically, two stages with respect

Department of Chemical Engineering, Faculty of Chemistry and Pharmacy, Sofia University, 1 J. Bourchier Ave., 1164 Sofia, Bulgaria. E-mail: SC@LCPE.UNI-SOFIA.BG; Fax: +359 2 962 5643; Tel: +359 2 962 5310

† Electronic supplementary information (ESI) available. See DOI: 10.1039/c3ra44500c

to water evaporation are reported:[9–13] (1) constant rate period (CRP) in which the evaporation rate is highest and most of the suspension shrinkage is observed[12,13] and (2) falling rate period (FRP) in which the water evaporation rate is reduced, due to the water diffusion within the sample, and very small shrinkage is observed in comparison to CRP (typically less than 15% of the total shrinkage). These two periods are separated by the so called "critical point" at which the sample shrinkage is strongly suppressed, as the particulate network "stiffens" and becomes able to resist the high capillary pressures occurring in the process of drying.[3,6,20]

In a detailed study of the process of drying of packed granular materials, Coussot[23] reviewed the main experimental and theoretical results from previous papers[24–29] and demonstrated convincingly the existence of three distinct regimes of drying, depending on the relative importance of (i) liquid evaporation from the surface of the porous material, (ii) liquid evaporation from the interior of the porous material, and (iii) capillary effects which are able to transport the impregnating liquid toward the surface of the porous material and inside its interior. These regimes appear as consecutive stages in the drying process of porous materials.[23–34] However, the boundary between two of these stages is not clearly seen when the total weight of the porous sample (liquid plus solid) is plotted as a function of time. In the latter plot, the second and the third stage of evaporation cannot be discerned easily and the evaporation appears as a two-stage process, as reported by most of the investigators. The physical origin of the three stages, reported in ref. 23, is explained in Section 3.1 below. Note that relatively homogeneous, non-shrinking porous materials were analyzed in ref. 23 – therefore, the model of Coussot should be further elaborated to describe the properties of shrinking drying foams, like those studied in the current paper.

Many studies show that the total level of shrinkage could vary significantly and might be as low as part of percentage for chemically settled systems,[35] while it could go up to 85% for wet gels/foams during conventional drying and sintering.[14] The impact of various factors on the shrinkage and total porosity of the dried materials was studied both experimentally and theoretically.[3,7] Krokida and Maroulism[7] studied the effect of the drying methods on the shrinkage and porosity of different fruits. Methods used in their study included conventional, vacuum and microwave drying, osmotic dehydration and freeze drying. They showed that all methods, beside freeze drying, lead to similar final results for both the shrinkage and the final porosity of the products.[7] These results were confirmed for particle stabilized foams by the group of Gonzenbach *et al.*[3] who compared conventional drying at different temperatures and freeze drying.

Recent reviews on the effect of drying temperature and air humidity were published by Katekawa and Silva,[15] Khalloufi *et al.*,[16] Kowalski and Pawlowski.[17] It was shown that the samples dry with fewer cracks at lower temperatures, higher humidity and unidirectional drying. Effect of pH on the structure of dried gels was discussed by Brinker and Scherer[6] on the basis of publications by Kawaguchi *et al.*[12] and Yamane *et al.*[18] They showed that silica xerogels shrink and crack less when prepared under alkali conditions which is explained with the different interactions between the particles in the drying suspensions. Similar results were obtained in the presence of surfactants.[19] This effect of surfactants was attributed to the decreased capillary pressure between the particles during drying.[20] Scherer[20] discussed also that the presence of electrolyte might have an impact on the drying kinetics of the samples, through a gradient of the osmotic pressure developed in the process of drying. A study published recently by Rad and Shokri[21] showed that salts indeed change the evaporation rate of water. The salts were found to have a significant impact on the mechanical integrity of the porous gels in some cases[22] in which salt crystallization may occur.

Several empirical and theoretical models were proposed to account for the shrinkage effects on the porosity of the drying systems, depending on the experimental conditions (see the reviews by Katekawa and Silva,[15] and Madiouli *et al.*[8]). All presented models, however, account only for very low (below 20% air) or no initial porosity of the wet precursor. The presence of initial cavities in the drying system, such as pre-dispersed bubbles, was not taken into consideration. Therefore, these models are not directly applicable to particle-stabilized foams and the question how to describe the shrinkage during drying of these specific systems is open.

The major aims of the current study are (1) to perform a coherent set of experiments on drying of particle-loaded aqueous foams in order to understand better the drying mechanism of these systems, and on this basis, (2) to develop a theoretical model for predicting the shrinkage and the final mass density and porosity of the obtained dry porous materials, before their possible post-processing which may include hydrophobization, sintering at high temperature, loading with catalytic nano-particles, *etc.* As we show below, the shrinkage process and the final properties of the porous material can be described by a simple set of equations, derived by considering the mass balances of particles, water and air in the sample, and the main regimes of drying, as described in ref. 23.

The structure of the paper is the following: Section 2 presents the materials and methods used. In Section 3, the main drying regimes of the porous materials are briefly described (following the ideas from ref. 23) and an explicit theoretical model, relating the properties of the foam precursor with the properties of the final porous material, is proposed. Two other possible theoretical models are also defined (see also the ESI Materials section†). Section 4 presents the main experimental results and their comparison with the theoretical models. Section 5 describes and explains the main stages of foam evolution during its drying and transformation into porous material. Section 6 summarizes the main conclusions of the study. The used notation is listed at the end of the text.

2. Materials and methods

2.1. Materials

Commercial powder of amorphous precipitated silica particles with concentration ≥87% (Tixosil 365, Rhodia) was used as particle source. According to its producer, the humidity loss

from this powder is 7 wt%, as determined by ISO 787/2 method (2 h at 105 °C). The ignition loss is 11 wt% determined by ISO 3262/11 method at 1000 °C. Along with particles, the product contains 1.5 wt% of soluble salts, determined by ISO 7888 method. The mean particle diameter provided by the manufacturer is $d_{50} \approx 3.5$–4 μm.

For the mass balance calculations below we assume that the original Tixosil powder contains 87.5 wt% particles with mass density of 2100 kg m^{-3}, and NaCl as inorganic salt with concentration of 1.5 wt% and mass density of 2165 kg m^{-3}. The physically bound water in the powder is 7 wt% with mass density of 997 kg m^{-3} (25 °C), while the remaining 4 wt% are for chemically bound water with (assumed) mass density of approx. 997 kg m^{-3}.

Two surfactants were used to modify the silica particles and to improve foam stability. Unfortunately, they could not be currently disclosed as they are a trade secret of the company funding this study. They would be denoted as surfactant 1 and 2 in the text below. For preparation of all solutions and suspensions, deionized water was used, as produced by Elix 3 module (Millipore Ltd.).

Highly viscous silicon oil (WACKER® AK 10 000, Wacker Silicones) was used in some of the measurements of the mass density of the dry porous materials, see Section 2.2.3 below. This oil has a dynamic viscosity of 10 000 mPa s and density of *ca.* 970 kg m^{-3}.

2.2. Methods

Porous materials were prepared through direct foaming of silica–surfactant suspensions at pH = 8.5. Two surfactants were used to check whether the surfactant type has influence on the properties of the final porous material. After preparation, the wet foam samples were dried at ambient conditions and their mass and volume were measured to determine the final mass density of the porous material and the volumetric shrinkage during drying – see below for the respective procedures.

2.2.1. Suspension preparation. Silica suspensions with pH = 8.5 were prepared in the following way: the necessary mass of silica particles was weighted in a polyethylene jar and deionized water was added. The suspension was homogenized on a ball mill drive (BML-2, Kugelmühlen-Antrieb) at 150 rpm for 30 min with glass balls of 7 mm diameter. Afterwards, this suspension was further homogenized for 2 h with a pulse sonicator (SKL-650W, Syclon). Sonicator was set to 1 s long pulses, separated by 0.5 s off periods, and power output of 450 W was applied, using a sonotrode with 10 mm diameter. The suspension pH was adjusted to 8.5 by addition of the necessary amount of 2 M NaOH and the suspension was homogenized again for 5 min with the ball mill and 60 min with the sonicator. Surfactant 1 or 2 was added to the silica suspension just before foaming.

The surface tensions of the surfactant solutions before mixing them with the silica suspensions were between 31 and 37 mN m^{-1} and depended weakly on the surfactant concentration, because these solutions were above the critical micelle concentration (CMC) of the surfactants. The surface tensions of the aqueous phases, separated by centrifugation of the particle suspensions, were 70.5 mN m^{-1} for suspension without surfactant (almost equal to that of pure water), 32.5 mN m^{-1} for surfactant 1 (*i.e.*, the surfactant in the aqueous phase was still above its CMC), and around 60 mN m^{-1} for surfactant 2 (*i.e.*, most of this surfactant was adsorbed on the particle surface, so that its concentration in the aqueous phase was below its CMC).

2.2.2. Foam generation. Powerful planetary mixer (Kenwood Chef Premier KMC 560, 1000 W) was used for the foam generation. The mixer was set to maximum speed until certain volume of foam was generated by air entrapment from the atmosphere. Then the mixer was stopped and the obtained sample was transferred into a Petri dish with known volume ($V_{F0} = 28$ mL ± 2%) to measure the foam mass, m_{F0}. The initial foam air volume fraction, Φ_0, was calculated from the measured foam mass using the equation:

$$\Phi_0 = 1 - \frac{V_{S0}}{V_{F0}} \quad (1)$$

where V_{S0} is the initial volume of the suspension, from which the foam is made, and V_{F0} is the initial foam volume. The notation φ_{P0} is used for the initial mass fraction of the particles in the suspension, which is defined as:

$$\varphi_{P0} = \frac{m_P}{m_P + m_{SP} + m_{WO}} = \frac{m_P}{m_{F0}} \quad (2)$$

where m_P is the mass of the silica particles in the foam (it does not change during foam drying), m_{SP} is the mass of the salt, which comes from the particles (it also does not change during drying), while m_{WO} is the initial mass of the water in the foamed suspension. As usual, the mass of the foam is assumed to be equal to the mass of the suspension, from which this foam is prepared, because the mass of the entrapped air is negligible. The ratio $m_{SP}/m_P \approx 1.5/87.5 = 0.01714$ is fixed in our experiments from the commercial composition of the used particle source (Tixosil 365). Assuming that the suspension volume is equal to the volume of the particles, salt and water, we can write:

$$V_{S0} = \frac{m_{WO}}{\rho_W} + \frac{m_P}{\rho_P} + \frac{m_{SP}}{\rho_S} \quad (3)$$

where ρ_W, ρ_P and ρ_S are the mass densities of water, particles and salt, respectively. Expressing m_P and m_{WO} as a function of m_{F0} and φ_{P0} from eqn (2) and substituting into eqn (3) we can determine V_{S0} as a function of m_{F0} and φ_{P0} and after substituting into eqn (1) we derive:

$$\Phi_0 = 1 - \beta(\varphi_{P0})\frac{m_{F0}\varphi_{P0}}{V_{F0}} \quad V_{F0} = \frac{\beta(\varphi_{P0})m_P}{1 - \Phi_0} \quad (4)$$

where $\beta(\varphi_{P0})$ is a physical parameter which has the meaning of a specific suspension volume per gram of particles in the suspension:

$$\beta(\varphi_{P0}) = \frac{V_{S0}}{m_P} = \frac{V_{S0}}{\varphi_{P0}m_{F0}} = \frac{1}{\rho_P} - \frac{1}{\rho_W} + \frac{m_{SP}}{m_P}\left(\frac{1}{\rho_S} - \frac{1}{\rho_W}\right) + \frac{1}{\varphi_{P0}\rho_W} \quad (5)$$

Note that φ_{P0} denotes the mass fraction of particles in the original suspension, as used in the foaming process. During the subsequent drying of the foams, the water evaporation reduces

the total mass of the foam which leads to related increase of the mass fraction of particles in the foam – this increasing mass fraction is denoted hereafter as $\varphi_P(t)$.

The air volume fractions, determined by eqn (1), were highly reproducible for foams with $\Phi_0 > 0.35$, with statistical error less than 0.02. For $\Phi_0 < 0.35$, the statistical error could reach up to 0.05. Therefore, only foams with $\Phi_0 > 0.35$ are considered in this study.

2.2.3. Foam drying. After determining Φ_0, foam samples with size 5–8 cm in diameter and 2–3 cm in height, were left to dry under ambient conditions – room temperature of 28 ± 5 °C and $40 \pm 10\%$ humidity. The containers with foams were loosely covered with a piece of filter paper to reduce the drying rate of the samples. Afterwards, they were left to dry for 2–3 weeks, until constant mass of the obtained porous materials was reached. No special drying conditions were applied because control experiments showed that the studied properties of the final dry porous materials practically did not depend on such variations of the drying conditions. The mass density of the dried samples was determined gravimetrically with accuracy of 0.01 g. The sample volume was measured by two different methods: (1) Vernier caliper method and (2) Archimedes method.

Vernier caliper method. The diameter, d, and height, h, of the porous materials were measured after drying with an accuracy of 0.5 mm. Some of the samples were slightly deformed during drying, so their diameter and height were averaged from several independent measurements in different directions. The sample volume was determined from the geometrical relation:

$$V_{PM} = \frac{\pi h d^2}{4} \pm 9\% \quad (6)$$

where ±9% is the estimated maximum error in this type of measurement.

Archimedes method. Pieces from the dry samples with known mass were placed in a 50 mL graduated cylinder and then silicone oil AK 10000 (WACKER®) with known mass was poured gently over the sample. This viscous oil was chosen not to allow the sample to float during the experiment, as well not to fill in rapidly the sample pores (as do the low viscosity oils or water). The sample volume was determined from the equation:

$$V_{PM} = V_{Total} - \frac{m_{SilOil}}{\rho_{SilOil}} \quad (7)$$

where m_{SilOil} and ρ_{SilOil} are the mass and the mass density of the used silicone oil, while V_{Total} is the sum of the volume of the porous material and the added silicone oil.

The difference between the results obtained by these two methods was found to be less than ±5% from 10 independent measurements of various samples. Therefore, the easier Vernier scale method was used for the systematic measurements described below.

After the sample volume was determined, the mass density of the porous materials, ρ_{PM}, and the volumetric shrinkage, K, were calculated using eqn (8) and (9):

$$\rho_{PM} = \frac{m_{PM} \pm 1\%}{V_{PM} \pm 9\%} \quad (8)$$

$$K = \frac{(V_F \pm 2\%) - (V_{PM} \pm 9\%)}{(V_F \pm 2\%)} \quad (9)$$

The measurement error for all of the studied systems was estimated to be around 10% for the mass density of the materials and <15% for their volumetric shrinkage.

2.2.4. Optical observations. Microscope observations of drying foams were performed to verify the proposed mechanism – see Section 4 below. Foams with known initial bubble volume fraction, Φ_0, and initial particle mass fraction in the aqueous phase, φ_{P0}, were prepared by the procedure from Section 2.2.2. These foams were transferred in a Petri dish with 5 cm diameter and 2 cm height. The uppermost layer of bubbles, in contact with the atmosphere, was observed in reflected light with microscope Axioplan (Zeiss, Germany) equipped with a long-distance objective Zeiss Epiplan 20×/0.40, CCD camera, video-recorder and monitor. Under these conditions, the foam films between the bubbles and the atmosphere appear as separated circular or elliptical regions, whereas the thicker Plateau channels around these films appear as brighter interconnected regions. The size of the individual bubbles could be estimated from such images by measuring the projected area of each bubble, A_i (the subscript i denotes the number of the observed bubble). The following formula is used, $R_i(t) = (A_i(t)/\pi)^{0.5}$, to estimate the radius R_i of the observed bubbles. We used the video records to determine the change in the size of the observed bubbles in drying foams. Bubble volumetric shrinkage was determined, as a function of time, and compared to the shrinkage of the respective macroscopic sample.

3. Theoretical models

3.1. Main regimes of convective drying of porous material

As demonstrated by Coussot[23] one can define three regimes of drying of the porous materials, depending on the relative importance of the surface evaporation, capillary transport of liquid, and evaporation from the interior of the porous sample.

In the first regime, the evaporation from the surface of the porous sample is dominating. The water leaving the porous material is replaced by air entering from the surrounding atmosphere. The experimental data and the theoretical analysis showed[23] that the entering air is not trapped around the surface of the porous material, but it rather penetrates deep into the sample by filling the largest pores in the material. Thus the area of the liquid surface in close proximity to the walls of the material remains almost constant and, therefore, the rate of liquid evaporation remains also relatively unchanged. This period of constant evaporation rate (called also "funicular regime" due to the continuous transport of liquid from the interior toward the surface of the sample) is characterized with the existence of a continuous liquid network throughout the entire sample.

The second regime occurs when the largest pores in the sample are filled with air, so that the major fraction of the pores at the sample surface becomes comparable in diameter to the major fraction of pores inside the sample interior. In this stage, part of the sample surface becomes depleted of liquid and, as a

result, the liquid close to the surface breaks into discontinuous wet patches. During this stage, the capillary pressures inside the pores increase and lead to redistribution of the liquid inside the interior of the sample, as a result of the capillary suction effects of the smaller pores. This stage appears in the drying kinetics as the "first decreasing rate period".

In the "second decreasing rate period" the liquid breaks into separate patches inside the liquid interior as well (so-called "pendular regime"). Here the extensive liquid redistribution, caused by the capillary effects, is halted and a completely dry front slowly recedes from the surface of the sample towards its interior, as a result of liquid evaporation from the separated liquid pools.

As we will see below, these three regimes could be seen in our experiments with drying foams. However, the original analysis of Coussot[23] is performed for non-shrinking, relatively homogeneous granular materials. As a result, in this analysis all air, needed to replace the evaporating water, is coming from the external atmosphere. In contrast, we have shrinking foams, containing bubbles with high volume fraction (above 0.5). Therefore, our system differs in two important aspects from the systems considered in ref. 23: (1) appropriate mass balance of the particles and water should be defined to account for the sample shrinking; (2) the possible replacement of the evaporating water by air from both the external atmosphere and the entrapped air bubbles should be considered. Therefore, the approach from ref. 23 is further modified in the following Sections 3.2 and 3.3 to account for these two additional effects.

3.2. Mass balance of water and particles in shrinking porous material

Any theoretical model should include a rigorous mass balance of the water and of the solid particles in the drying shrinking material, as briefly described in this section.

The mass of the porous materials after drying, m_{PM}, is equal to the mass of the foam structural elements that contain particles after drying. For brevity, the various structural elements of the foams which may contain particles after drying (nodes, Plateau channels and foam films) are called "foam walls" in the following consideration.

$$m_{PM} = m_{wall} = \rho_{wall} V_{wall} \tag{10}$$

here V_{wall} is the volume of foam walls and ρ_{wall} is the average mass density of the dry foam walls. ρ_{wall} is assumed to be constant for a given sample (on average) and depends on the particle close packing after drying (see Fig. 6 below for justification).

Combining eqn (8) and (10) we derive the following equation for the final mass density of the porous material:

$$\rho_{PM} = \frac{m_{PM}}{V_{PM}} = \frac{m_{PM}}{\frac{m_{PM}}{\rho_{wall}} + V_{BD}} \tag{11}$$

where V_{BD} is the volume of the bubbles in the final dry material. More precisely, V_{BD} is the volume of pores in the final dry material which is inherited by the bubbles in the initial wet foam. Taking into consideration eqn (4), (9) and (11), one derives the following equation for foam shrinkage:

$$K = \frac{V_{F0} - V_{PM}}{V_{F0}} = 1 - \frac{\left(\frac{m_{PM}}{\rho_{wall}} + V_{BD}\right)}{\frac{\beta(\varphi_{P0}) m_P}{1 - \Phi_0}} \tag{12}$$

where V_{F0} is the initial foam volume, V_{PM} is the volume of the final porous material, Φ_0 is the initial bubble volume fraction in the foam, m_P is the mass of the particles. Eqn (11) and (12) are simple mass balance equations and do not allow us to predict when the shrinkage of the sample would stop. Therefore in the following Section 3.3 we use additional assumptions about the changes in the foam structure, in the process of drying, in order to obtain a complete set of equations describing the relations between the initial wet foam and the final dry porous material.

3.3. Final mass density and degree of shrinkage of the final porous material

To complete the set of eqn (11) and (12) we have to define two (still unknown) independent quantities – the final mass density of the foam walls, ρ_{wall}, and the volume of the bubbles in the final porous material, V_{BD}. As explained in Section 3.2 and proven in Section 4, we assume that ρ_{wall} is determined by the particle close packing after drying. However, it is not obvious in advance how to relate the initial bubble volume fraction in the wet foam, Φ_0, with the final volume of the bubbles in the dry porous material, V_{BD}. The main reason for this uncertainty is that the bubbles may shrink in the drying process (following the shrinkage of the entire sample) and, in addition, could provide air to fill the micro- and nanopores between the particles in the drying foam walls. Therefore, one must consider a mass balance of the air in the drying samples to complete the set of eqn (11) and (12). Three different possibilities for air redistribution are considered below, which are formulated as three theoretical models to be compared with the experimental results in Section 4.

As explained by Coussot[23] the capillary pressures developed in the process of drying of porous materials are sufficiently high to transport liquid from the bulk toward the surface of the material and inside the porous material. These pressures are of the order of σ/R_p where $\sigma \approx 30$ mN m^{-1} is the liquid surface tension and R_p is the pore radius. For nanometer sized pores, like those formed in our samples, these pressures could be as high as 10^7 Pa.

In the case of shrinking bubbled materials, like the foams studied here, we should compare these capillary pressures to the compression yield stress of the foam walls (which resists the sample shrinkage) and to the capillary pressure of the trapped bubbles. The bubble capillary pressure is of the order of $\sigma/R_B \approx 10^3$ Pa where $R_B \approx 10^{-4}$ m is the bubble radius. Thus we see that the capillary pressures developed in the pores are many orders of magnitude higher than the bubble capillary pressure. Estimating the compression yield stress is a more difficult task, because there are no simple theoretical models to account for the complex structure of the studied systems. Furthermore, in

the process of sample shrinking, the particles rearrange and acquire more compact structure inside the foam walls, which leads to a significant increase of the compression resistance. For all models considered below we assume that the foam shrinkage would stop when the foam wall density becomes equal to a given value ρ_{wall}, which corresponds to a sufficiently high yield stress, able to counterbalance the compressing capillary pressure.

The above estimates suggest that the shrinking process is driven and dominated by the high capillary pressures developed in the pores of the foam walls, while the capillary pressure of the bubbles has negligible effect. Therefore, in the first model of sample shrinkage we assume that the foam walls and the bubbles shrink equally during drying, *viz.*, affine shrinkage of the material is realized:

$$K = K_{wall} = \frac{V_{S0} - V_{wall}}{V_{S0}} \quad (13)$$

here K_{wall} is the shrinkage of the walls, V_{S0} is the initial volume of the suspension (the "continuous" phase) in the foam and V_{wall} is the volume occupied by the foam walls after drying. Under these assumptions we derive:

$$V_{BD} = (1 - K)V_{B0} = (1 - K)\Phi_0\beta(\varphi_{P0})m_P/(1 - \Phi_0) \quad (14)$$

The pores in the drying foam walls are filled by air coming from both the bubbles and the atmosphere. Under these assumptions, the following final equations are derived to describe the mass density and the shrinkage of the porous material:

$$\rho_{PM} = \rho_{wall}(1 - \Phi_0) \quad (15)$$

$$K = 1 - \frac{1}{\rho_{wall}\varphi_{PD}}\frac{1}{\beta(\varphi_{P0})} \quad (16)$$

here φ_{PD} is the mass fraction of the particles in the dried porous material. Reasonable assumption is that the walls in the final dry porous material have the same composition as the initial particle source, *viz.* $\varphi_{PD} = 0.875$. The rest is salts and bound water which may remain in the walls of the porous material when the latter is dried under ambient conditions.

Hereafter, we denote eqn (15) and (16) as "Model 1". According to this model, the mass density of the final dried materials depends on the initial bubble volume fraction, Φ_0, while the foam shrinkage is independent of Φ_0 but depends on the particle mass fraction in the initial suspension, φ_{P0} (Fig. 1A–D). For this model, the shrinkage stops completely if the initial foam is prepared from suspension with initial particle concentration of $\varphi_{P0} = 0.332$ when $\rho_{wall} = 460$ kg m^{-3} (see Fig. 1B and D). Much larger shrinkage is predicted by this model, as compared to the other two models (see Fig. 1B).

Although physically justified, Model 1 is not the only theoretical construction one could define for the process studied. In the ESI† we define two other models which differ mainly in the

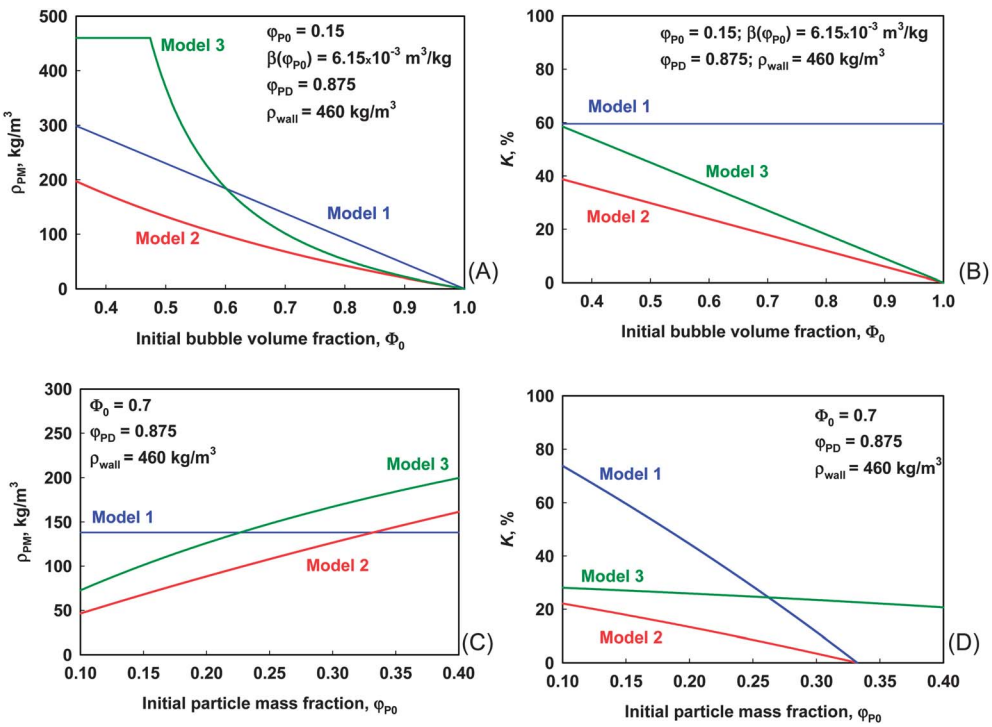

Fig. 1 Predictions of the three theoretical models for the final mass density and the shrinkage during drying of the porous materials. (A) Mass density and (B) shrinkage of the materials, as functions of the initial bubble volume fraction in the wet foam, Φ_0, for initial particle mass fraction in the suspension, $\varphi_{P0} = 0.15$; (C) mass density and (D) shrinkage of the materials, as functions of φ_{P0} for foams with initial bubble volume fraction of $\Phi_0 = 0.70$. The curves represent the predictions of Model 1 (blue curves), Model 2 (red curves) and Model 3 (green curves). The final mass density of the wall is assumed to be 460 kg m^{-3} and the final mass density of the particles in the foam walls is 0.875, as we found in the experiments with dried suspensions (Section 4.2).

assumptions about the origin of air, needed to replace the evaporating water from the shrinking sample. One of these models assumes that all air is taken from the atmosphere (as in the case of non-shrinking samples) whereas the second model takes the other extreme, namely, that all air is taken from the bubbles initially trapped in the foam. These models are called hereafter "Model 2" and "Model 3".

Model 2 is based on the assumption that the evaporating water is replaced by air from the atmosphere only, while the bubble volume remains constant during drying. Then the following expressions for the mass density of the final porous material and for its degree of shrinkage are derived (see ESI†):

$$\rho_{PM} = \frac{1}{\frac{1}{\rho_{wall}} + \frac{\Phi_0}{1-\Phi_0}\beta(\varphi_{P0})\varphi_{PD}} \quad (17)$$

$$K = (1-\Phi_0)\left(1 - \frac{1}{\rho_{wall}\varphi_{PD}}\frac{1}{\beta(\varphi_{P0})}\right) \quad (18)$$

This model predicts a gradual decrease of the mass density of the dry samples with the increase of bubble volume fraction in the wet foam, Φ_0, at given particle concentration in the initial suspension (see Fig. 1A) and an increase of the sample mass density with the increase of particle concentration at constant Φ_0 (Fig. 1C). The shrinkage should depend both on the initial particle concentration, φ_{P0}, and on the initial air volume fraction, Φ_0.

Model 3 is based on the assumption that the evaporating water in the foam walls is preferentially replaced by air taken from the bubbles. Under this assumption, the mass density of the final porous material and the shrinkage of the samples are described by (see ESI†):

$$\rho_{PM} = \frac{1}{\Phi_0\beta(\varphi_{P0})\varphi_{PD}/(1-\Phi_0) - (\varphi_{PD}/\varphi_{P0}-1)/\rho_w + 1/\rho_{wall}} \quad (19)$$

$$K = (1-\Phi_0)\left(\frac{1}{\varphi_{P0}} - \frac{1}{\varphi_{PD}}\right)\frac{1}{\rho_w\beta(\varphi_{P0})} \quad (20)$$

This model predicts a linear decrease of K with the increase of air volume fraction, at fixed initial particle concentration (Fig. 1B).

As seen from Fig. 1, Models 1–3 predict very different dependences of ρ_{PM} and K on φ_{P0} and Φ_0. The latter fact allows one to check these models by comparing their predictions to experimental data for foam shrinkage during drying.

4. Experimental results and data interpretation

In the current section, results from the experiments on drying and shrinkage of particle-stabilized foams are presented and compared to the theoretical models. The effects of particle concentration and bubble volume fraction are investigated systematically. Several additional series of experiments were performed to demonstrate that the surfactant type and concentration had minor effect on the process of drying.

4.1. Stages of foam drying

Experimental results for the kinetics of drying and shrinkage of particle-stabilized foam are presented in Fig. 2. In this experiment, foam with $\Phi = 0.78$ and $\varphi_{P0} = 0.158$ was prepared in the presence of 6.6×10^{-2} wt% surfactant 2 at pH 8.5. Linear decrease of the foam mass with time was observed during the first $\approx$ 500 min, see Fig. 2A. During this period, no shrinkage of the foam was observed, *cf.* Fig. 2A and C. Afterwards, gradual decrease of the drying rate was observed until a constant foam mass was reached after >6000 min (100 h). The final mass of the dry material corresponded precisely to the amount of Tixosil 365 which was introduced initially in the sample (silica particles, salt and water coming from the particles), so the whole amount of water added to prepare the silica suspension was evaporated and the final mass fraction of silica particles in the dried material is 0.875, see Fig. 2B. During the second period (the falling rate period), significant shrinkage of the foam was observed – see Fig. 2C. This shrinkage was close to linear in the main period, from *ca.* 500–1800 min, and continued more slowly from 1800 to 2800 min. The total volumetric shrinkage was around 60% and it stopped well before the entire water was evaporated from the sample, *cf.* Fig. 2B and C.

Note that these results with foams differ in one very important aspect from the results reported in literature for drying particulate gels – the gels were shrinking predominantly during the initial "constant rate period", whereas we observe a very clear "induction" period before the shrinking starts. Qualitative explanation of the shape of the shrinkage curves, like that shown in Fig. 2C is given in Section 5 below.

4.2. Comparison with the theoretical models

As one can see from the model predictions, one of the main differences between the proposed models is the dependence of the foam shrinkage on the initial bubble volume fraction, see eqn (13–20) above. Models 2 and 3 predict that the shrinkage depends significantly on the initial bubble volume fraction, whereas Model 1 predicts that the shrinkage does not depend on Φ_0, see Fig. 1A. To compare the experimental results with the model predictions, several foams with different bubble volume fractions were first prepared, at fixed concentrations of silica particles and surfactant. Representative results from these experiments are shown in Fig. 3, where the shrinkage of foams with particle mass fraction in the initial suspension $\varphi_{P0} = 0.158$, in presence of 6.5×10^{-2} wt% surfactant 2, was studied at $\Phi_0 =$ 0.57; 0.78 and 0.87. The shrinkage is presented in Fig. 3A as a function of the particle mass fraction in the sample during drying, $\varphi_P(t)$. This fraction increases as water evaporates from the sample *via* the following mass balance:

$$\varphi_P = m_{P0}/m_F(t) \quad (21)$$

here m_{P0} is the initial mass of the silica particles and $m_F(t)$ is the total mass of the foam, measured at moment t. As seen from Fig. 3, the three samples exhibited very similar trends – initial induction period with no shrinkage, then relatively rapid shrinkage, and finally a constant foam volume was reached,

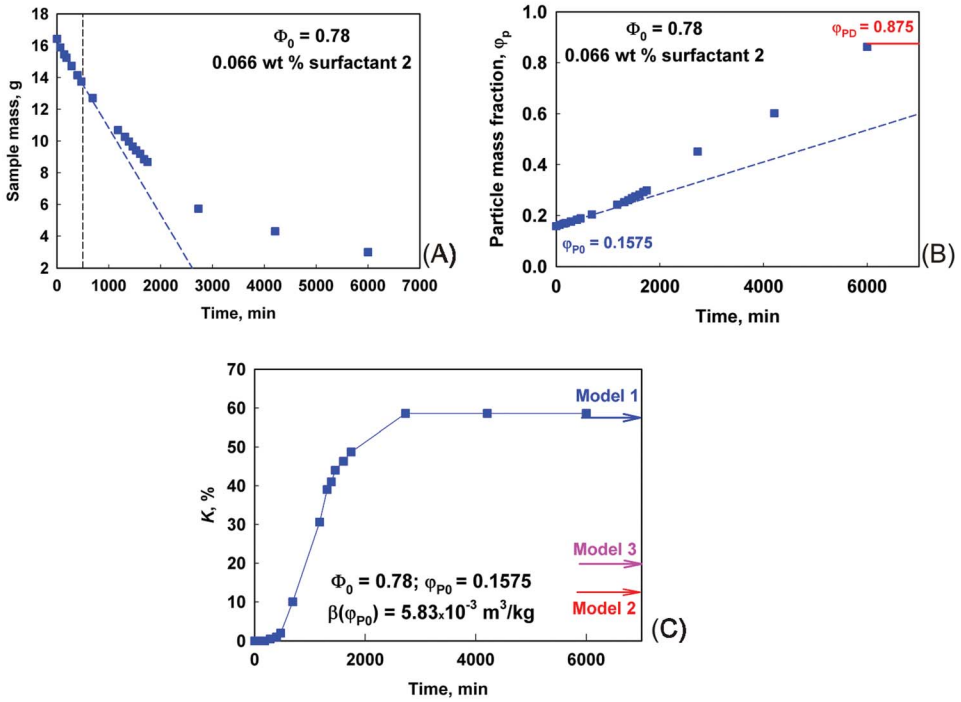

Fig. 2 Experimental results for drying of particle-stabilized foam with initial bubble volume fraction $\Phi_0 = 0.78$, and initial particle mass fraction $\varphi_{P0} = 0.1575$. The foam is formed in presence of 0.066 wt% surfactant 2 in the aqueous suspension. Kinetics of (A) foam mass decrease; (B) particle mass fraction increase and (C) sample shrinkage as functions of drying time. The dashed curves are guides to the eye, whereas the arrows show the predictions of the sample shrinkage by Model 1 (blue arrow); Model 2 (red arrow) and Model 3 (pink arrow). For the theoretical calculations $\rho_{wall} = 460$ kg m^{-3} is assumed.

although the water was still evaporating from the sample (while φ_P was increasing in the foam walls from 0.4 to 0.875). The differences in the shrinkage of the different foams was negligible and within the experimental error. Illustrative images of dried foams with the same initial volume are shown in Fig. 3B and C for samples with $\Phi_0 = 0.57$ and 0.78, respectively. Samples before drying had a diameter of 7.5 cm and shrunk after full drying to *ca.* 5.8 cm for both samples. The volumetric shrinkage was $K \approx 60\%$, *i.e.* the samples shrunk to $\approx$40% of their initial volume. The results about the total shrinkage of these samples are in a very good agreement with the values predicted by Model 1, whereas the other models predict different shrinkage levels, see the red lines in Fig. 3.

It is worth noting that all these samples stopped shrinking at a specific particle mass fraction in the drying foam $\varphi_P \approx 0.33$. To investigate this observation in more details, we prepared foams with the same bubble volume fraction, but with different particle concentrations in the foamed suspension. Fig. 4 represents the shrinkage as a function of φ_P for these samples The presented data are for initial particle mass fractions of $\varphi_{P0} = 0.121$; 0.158 and 0.241. Both initial wet foams had bubble volume fraction $\Phi_0 = 0.57 \pm 0.03$. Again S-shaped curves were observed for the sample volume *vs.* time, see Fig. 4. Shrinkage was faster and greater for the sample with lower initial concentration of particles. The final shrinkage was about 75% for $\varphi_{P0} = 0.121$ and about 31% for foam with $\varphi_{P0} = 0.241$. The values predicted by Model 1 are in relatively good agreement, 68% and 33%, respectively, whereas the other models predicted much lower shrinkage. In both cases, the shrinkage stopped at around the same final concentration of particles ($\varphi_P = 0.33 \pm 0.05$). Therefore, this particle concentration corresponds to the maximum packing of the particles in the foam walls during drying.

To check whether the theoretical Model 1 is applicable to foam samples, containing different surfactants, we investigated the kinetics of shrinkage of foams containing surfactant 1 or 2. Fig. 5 represents the shrinkage of the samples as a function of φ_P. The presented data are for $\varphi_{P0} = 0.158$, in the presence of 0.50 wt% surfactant 1 or 0.10 wt% surfactant 2. For both samples no shrinkage was observed during the initial period. Afterwards, there was a rapid shrinkage until plateau region for the foam volume was reached. The final shrinkage was about $60 \pm 3\%$ for both samples, despite the different types and concentrations of surfactant used. One should note that the shrinkage stopped again at $\varphi_P = 0.33 \pm 0.05$ for both surfactants.

To check the aforementioned hypothesis about the role of the maximum particle packing density which prevents further shrinkage, and to study the effect of the surfactant type and concentrations on this final packing density, we performed model experiments by non-foamed suspensions of the same particles, in the presence and in the absence of surfactants. Surfactant 1 or 2 was added to the silica suspensions which contained particles with $\varphi_{P0} = 0.131$. After adding the

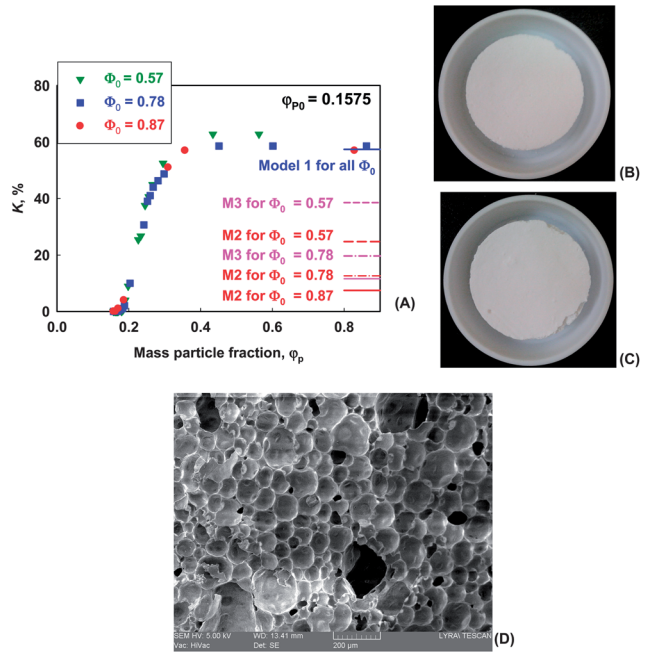

Fig. 3 (A) Shrinkage as a function of particle mass fraction φ_P inside the sample during drying. Samples with initial $\varphi_{P0} = 0.1575$ at different initial bubble volume fractions, $\Phi_0 = 0.57$ (green triangles), 0.78 (blue squares) and 0.87 (red circles) are studied. The lines indicate the predictions of the three models described in Section 3 – Model 1 (blue lines); Model 2 (red lines) and Model 3 (pink lines) for samples with different volume fractions of 0.57 (dashed lines); 0.78 (dashed-dot lines) and 0.87 (continuous lines). Note that Model 1 predicts the same shrinkage for all samples with different initial bubble volume fractions. Pictures of the foams after drying for (B) $\Phi_0 = 0.57$ and (C) $\Phi_0 = 0.78$, and (D) SEM image for sample with $\Phi_0 = 0.78$. Diameter of the dry samples is 5.8 cm, whereas the internal diameter of the Teflon mold is 7.5 cm.

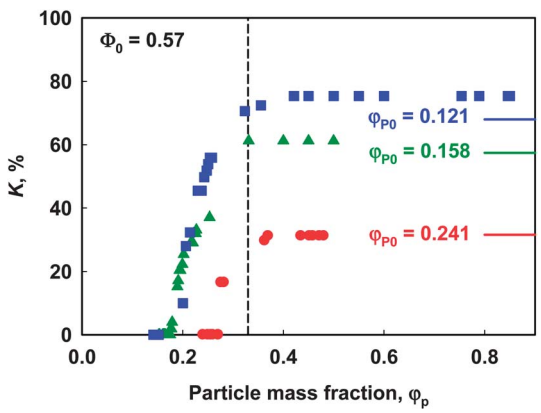

Fig. 4 Shrinkage as a function of φ_P inside the sample during drying, for foams formed from initial suspension with $\varphi_{P0} = 0.121$ (blue squares); $\varphi_{P0} = 0.158$ (green triangles) and $\varphi_{P0} = 0.241$ (red circles). The three samples are with initial bubble volume fraction of $\Phi_0 = 0.57 \pm 0.03$. There is a final particle concentration in the foam walls (denoted by the vertical black line) above which no shrinkage is observed. The horizontal lines show the predictions for the final compaction of these samples, based on Model 1.

surfactant, the suspensions were mixed very gently to avoid any air entrapment. Afterwards they were dried at ambient conditions and their mass densities were measured and compared.

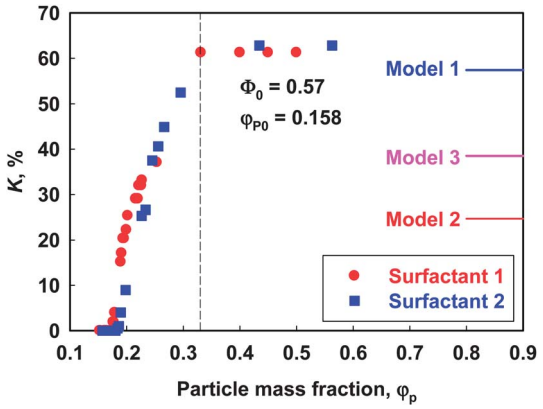

Fig. 5 Shrinkage as a function of φ_P inside drying samples with initial particle mass fraction $\varphi_{P0} = 0.158 + 0.5$ wt% surfactant 1 (red circles) or + 0.10 wt% surfactant 2 (blue squares), at initial bubble volume fraction $\Phi_0 = 0.57 \pm 0.02$. The three lines indicate the predictions of the theoretical models from Section 3.

During drying, these suspensions broke into small pieces, so shrinkage of the samples could not be measured very accurately (note that the respective foam samples did not break during drying). However, these small pieces could be used for determination of their mass density by the Archimedes method (Section 2.2.2). The obtained results are presented in Table 1. The mass density of the dried suspensions was around 460 ± 20 kg m^{-3} for all these samples, with and without surfactants. This means that the final packing of the particles depended primarily on their compaction under the action of the high capillary pressures in the drying samples, while parameters which do not affect his compaction (rate of water evaporation, type and concentration of surfactant, *etc.*) had secondary importance.

Another important result of this measurement was that the mass density of 460 ± 20 kg m^{-3} corresponds to about $\varphi_P = 0.33$ packing fraction of particles in the suspension. This result is rather close to what we observed as a value for the particle packing at the end of the compaction process of the drying foams (*cf.* Fig. 3–5) and it is also in a very good agreement with the value of ρ_{wall}, as determined from the fit of the theoretical Model 1 to the experimental data (see Fig. 6B below).

A comparison between the obtained experimental data and the theoretical predictions of the three models is presented in Fig. 6 for many different samples, varying in the surfactant type and concentration, particle mass fraction in the foamed suspension, and the bubble volume fraction in the wet foam. All

Table 1 Mass density of 13.1 wt% silica suspensions, dried at ambient conditions, in the presence and in the absence of surfactants

System	Surfactant concentration in the suspension, wt%	Density of the dried suspensions, kg m^{-3}
Suspension	0	462 ± 20
+ Surfactant 1	0.50–1.00	464 ± 20
+ Surfactant 2	0.10–0.25	460 ± 20
Average		462 ± 20

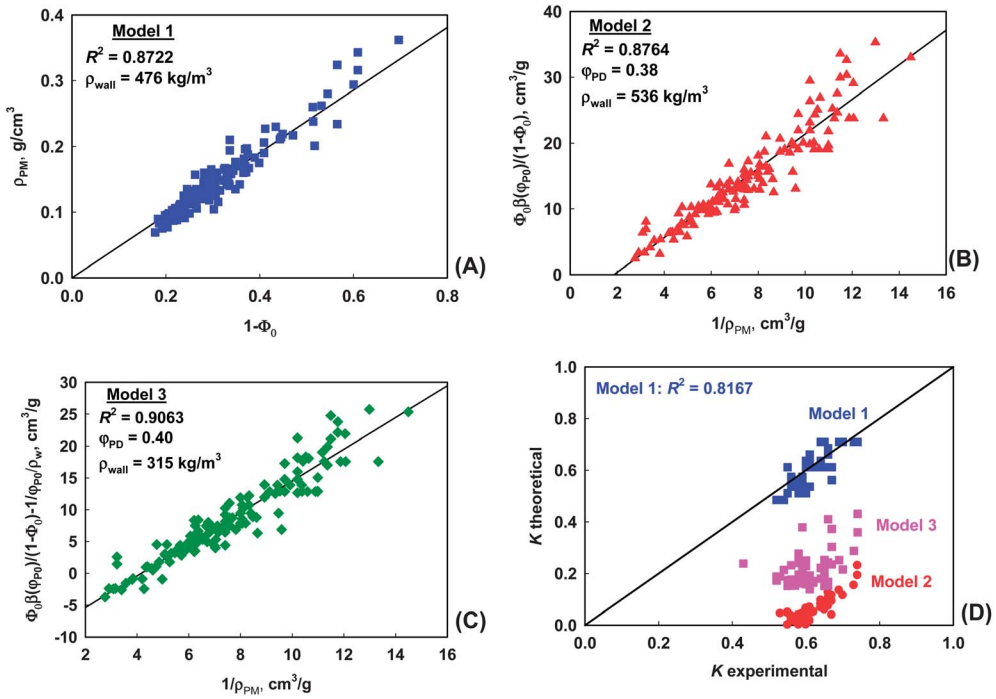

Fig. 6 Measured mass density of the final porous materials *vs.* the theoretical predictions of: (A) Model 1, (B) Model 2, and (C) Model 3 for 100 samples, differing in the initial particle concentration, bubble volume fraction, and type and concentration of surfactant in the foamed suspension. The straight lines represent the model predictions while the symbols represent experimental data. (D) Measured foam shrinkage *vs.* the predicted shrinkage for Model 1 (blue squares), Model 2 (red circles) and Model 3 (green circles). The correlation coefficients and the respective values for ρ_{wall} are indicated in the figures – these values are determined from the linear fits to the data and are different for Models 1 to 3.

three models describe the mass density of the porous materials reasonably well, if appropriate ρ_{wall} is assumed for each model. The experiments with drying silica suspensions (see Table 1) indicate that the most probable mechanism is the one encrypted in Model 1, as the mass density of the dry silica suspension is closest to the wall density needed to explain the foam data by this model (460 ± 20 kg m^{-3} measured and 477 kg m^{-3} from the theoretical fit). Even more decisive discriminator between the models is the foam shrinkage. Fig. 6D represents the three model predictions, as functions of the measured shrinkages. It is obvious that only Model 1 predicts such high shrinkages of the samples, as those observed experimentally.

4.3. Bubble shrinkage during foam drying

One feature of Model 1 is the prediction that the bubbles shrink inside the drying foam at the same level (on average), as the macroscopic sample. Optical observations of drying foams were performed to verify this prediction. Wet foams were prepared and transferred into two Petri dishes with the same volume. One sample was observed in reflected light during its drying to video-monitor the changes in the bubble size, whereas the other sample was used for measurements of the shrinkage of the macroscopic sample.

Bubbles volumetric shrinkage was calculated from the video records as a function of time (Fig. 7) and compared to the results obtained for the shrinkage of the macroscopic sample (Fig. 8). Results for the samples containing $\varphi_{P0} = 0.158 + 6.6 \times 10^{-2}$ wt% surfactant 2, at $\Phi = 0.83$; and $\varphi_{P0} = 0.206 + 8.6 \times 10^{-2}$ wt% surfactant 2, at $\Phi = 0.65$, are presented in Fig. 8A and B, respectively. One sees a very good agreement between the measured microscopic and macroscopic total shrinkages of the same samples. Furthermore, in the first stages of foam drying one sees an initial expansion of the bubbles, appearing as "negative shrinkage" of the bubbles (the empty symbols), which is easily explained in the frame of Model 1 – see Section 5 below. Therefore, we can conclude that Model 1 is the one that

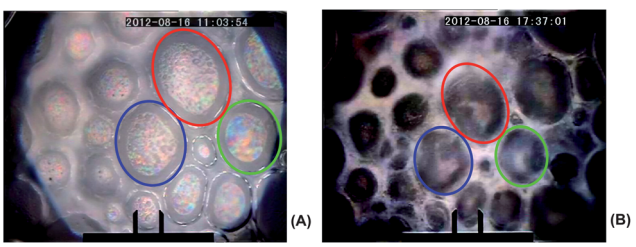

Fig. 7 Microscopic shrinkage of bubbles in a foam with initial particle mass fraction $\varphi_{P0} = 0.158 + 1.8 \times 10^{-2}$ wt% surfactant 2 (A) Immediately after foam preparation and (B) After 450 min of drying. The colored ellipses indicate the initial (in A) and the final sizes (in B) of the same bubbles. The volumetric shrinkage of the bubbles can be estimated from the projected bubble area, as explained in Section 2.2.4. In this particular experiment the projected area of the bubbles decreased by 51 ± 8% which corresponds to a volumetric shrinkage of these bubbles by 66 ± 10%. For comparison, the volumetric shrinkage of the respective macroscopic sample was 70%. The distance between the two vertical bars at the bottom of the image is 50 μm.

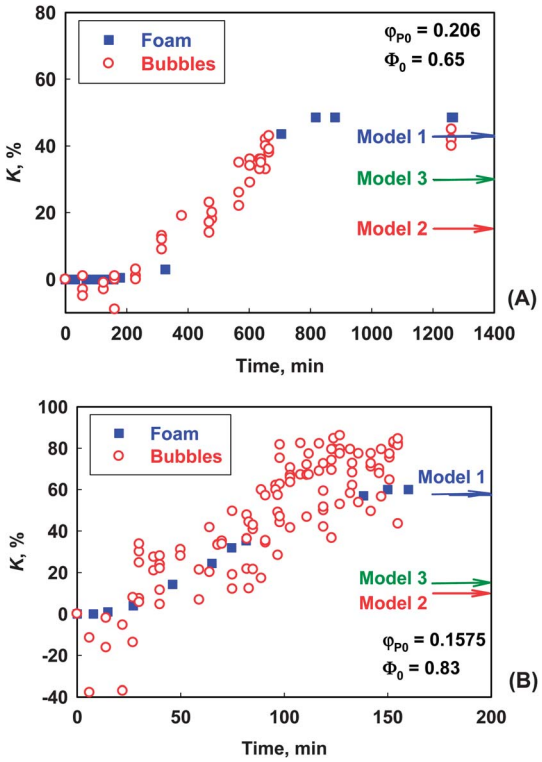

Fig. 8 Comparison of the macroscopic shrinkage of the foams (blue squares) and microscopic shrinkage of single bubbles in the same samples (empty circles), as functions of time for: (A) $\varphi_{P0} = 0.206 + 8.6 \times 10^{-2}$ wt% surfactant 2, at $\Phi_0 = 0.65$; and (B) $\varphi_{P0} = 0.158 + 6.6 \times 10^{-2}$ wt% surfactant 2, at $\Phi_0 = 0.83$. The arrows indicate the predictions of Models 1–3 for the overall shrinkage of the samples after drying.

describes very well all studied foams, stabilized by the studied surfactant-silica mixtures.

5. Mechanistic explanation of the observed stages of drying

The foaming of the silica–surfactant suspensions and their properties which are crucial for ensuring long-term foam stability, are two important aspects of the studied phenomenon, which are not discussed in this paper – they are analyzed in other studies[4,36] and, therefore, we focus here only on the subsequent stages of drying of the wet foam precursor. For the following discussion it is important to stress only that the foamed suspensions must have a certain yield stress, in order to suppress the gravity-driven drainage of the suspension from the wet foam which, otherwise, would destabilize the foam before and during drying.[36,37]

Let us summarize here the main stages of transformation of the silica-loaded aqueous foams into dry porous material, as observed in our study and compare these stages to the physical regimes of evaporation, as described in ref. 23 and Section 3.1. All our experimental data are described very well by eqn (15) and (16) in Model 1, and the following explanations implement the main assumptions of this model – see Fig. 9 for schematic presentation.

As seen from Fig. 2–5, the first stage of water evaporation does not lead to shrinkage of the wet foam. Because the foam is loosing around 20% of its mass during this stage (see Fig. 2A), the only way to explain this result is to assume that there is a local shrinkage and rearrangement of the foam walls inside the sample, in order to compensate for the lost volume of water which leaves the sample. This means also that the bubbles inside the foam should slightly increase their volume during this stage to compensate for the water loss. In addition, air could penetrate from the atmosphere into the bulk of the sample, *via* the largest pores in contact with the sample surface, to compensate for the water evaporation (as in the "funicular regime" of drying described in Section 3.1). These local rearrangements of the foam walls are triggered by the high capillary pressures which develop in the process of drying. Indeed, assuming that the pore size in the foam walls is similar to the size of silica agglomerates (several micrometers) we estimate that the local capillary pressures in this initial period of water evaporation could reach up to 10^7 Pa which is several orders of magnitude higher than the bubble capillary pressure.

This first stage of evaporation ends when the capillary pressure, created by the evaporating water in the pores of the foam walls, becomes sufficiently high to overcome the compression yield stress of the foam. In this moment the foam

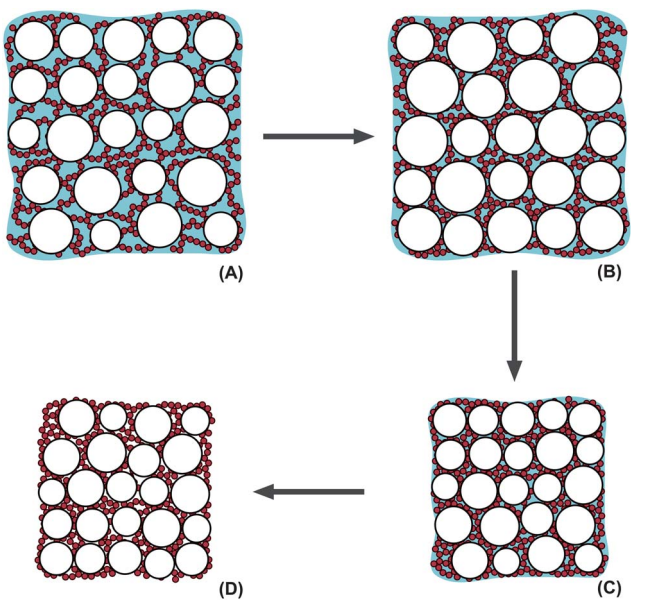

Fig. 9 Schematic presentation of the main drying stages of pre-foamed particle suspensions, as observed in our experiments (*cf.* with the experimental data in Fig. 2). (A → B) In the first stage, water evaporates without shrinking of the sample. The water loss is compensated by local rearrangement of the walls of the wet foam. (B → C) During the second stage the sample shrinks significantly, due to a compaction of the particles inside the wet foam walls, until a critical packing density of the particles is reached which resists the further shrinking. In our experiments, this critical particle packing was ≈ 33 wt % which corresponds to ≈23 vol% of fractal silica particles in the wet foam walls. (C → D) During the final stage, all water is evaporated (except for the water bound to the particles) without changing the sample volume and the final dry porous material is obtained.

starts to shrink, due to compaction of the particles in the foam walls, until the particles acquire a well packed structure, sufficiently strong to resist the compressing capillary forces which develop in the pores. It is rather possible that some of the silica agglomerates brake during this stage, under the action of the strong capillary pressures. Also the bubbles shrinkage in this stage follows the shrinkage of the foam walls (*viz.* of the entire foam sample) because the bubble capillary pressure which resists shrinkage, is several orders of magnitude lower than the capillary pressure developed in the foam walls by the evaporating water.

As seen from Fig. 2–6, the end of the second stage occurs when the mass fraction of particles in the wet foam walls becomes around 33%. Taking into account the mass densities of silica and water, we estimate that this moment corresponds to around 23 vol% of silica particles in the foam walls, for the used Tixosil sample. One should note that this very important parameter of the drying process may depend strongly on the particles used. If the particles are spherical, this close packing is expected to occur at around 60–80 vol%, depending on the polydispersity and the interactions between the particles. However, for highly porous fractal particles, like the silica used in our experiments, we see that the close packing occurs at 3-fold lower volume fraction of particles in the foam walls.

During the third stage, no sample shrinkage is observed although the rest of the water, added in the process of suspension preparation, is evaporated until the final dry material is obtained. We observed that the mass of the final product was exactly equal to the mass of the Tixosil powder, added in the foamed suspension. This means that the final porous material still contains around 11% chemically and physically bound water and 1.5 wt% salt, inherited from the original Tixosil powder. This final product has significant mechanical strength and might be further post-processed, *e.g.* to increase its mechanical integrity *via* sintering at high temperature and/or to modify the surface of its pores.

The comparison of Fig. 2A and C shows that the duration of the first (induction) period coincides with the period of constant water evaporation, both proceeding for $\approx$500 s. The following main period of sample shrinking, up to *ca.* 2000 s for this particular sample, is characterized with slowly decreasing rate of water evaporation. The final evaporation stage, between 2000 and 6000 s, is characterized with small or completely halted sample shrinkage and much lower evaporation rate. Similar consecutive stages, although with different durations and evaporation rates, were observed with the other foam samples studied. From these observations we may conclude that the three periods, observed with our shrinking foams, coincided with the three physical regimes of drying of porous non-shrinking materials, as described in Section 3.1. This conclusion is not surprising, because the same capillary pressures, which develop in the tiny pores between the particles, are able to transport liquid and to compress the particles inside the porous material, thus leading to shrinkage. Depending on the compression resistance of the particulate network in the porous material (compression yield stress), one or another of these two processes may prevail in a given moment.

6. Conclusions

A simple theoretical model (Model 1, see eqn (15) and (16)) is proposed in the current study to describe the process of drying of particle-stabilized foams. This model allows one to predict the total shrinkage of the foams after drying, as well as the final mass density of the obtained porous material from the properties of the wet foam precursor. Only one material parameter is required to make these predictions – the wall density of the dry mineral foams. In our study, this parameter was determined independently, *via* gravimetrical measurement of the mass density of the silica suspensions, used in the foaming experiments, after their complete drying.

Three stages of foam evolution during drying were experimentally observed, as shown in Fig. 2–5 and 9 – induction period, relatively rapid sample shrinking, and final water evaporation at constant volume of the sample. The observed stages are explained mechanistically by considering the main physical processes of convective drying of porous materials (Section 3.1) and accounting for the important role of the maximum packing density of the particles in the shrinking foam walls.

In agreement with the theoretical model, we observed affine shrinkage for the bubbles inside the foams and the foam walls, *viz.* the volumetric shrinkage of the bubbles is equal to the shrinkage of the entire sample, Fig. 7 and 8. The experimental results for the density and shrinkage of particle-stabilized foams are described very well by the model for a wide range of experimental conditions: air volume fraction of the wet foams varied between 0.35 and 0.83, particle mass fraction in the foamed suspension varied between 0.10 and 0.26, different types of surfactant 1 or 2, and at various surfactant concentrations (varied between 0.05 and 2.85 wt%).

Therefore, we expect that the observed stages (Fig. 2 and 9) and their theoretical description, eqn (15) and (16), are valid for a wide range of particle-loaded foams. Furthermore, the proposed model can be further elaborated to predict the pore size distribution in the final porous material, from the initial bubble size distributions and from the size distribution of the pores in dried particle suspensions (the latter should be measured in an independent experiment).

Acknowledgements

The authors are grateful to Miss Monika Kovadjieva from Sofia University for performing some of the foaming experiments, and to Dr David Louapre, Marie Lamblet, and Valerie Goletto (all from Saint Gobain Research, Paris) for the numerous useful discussions. The support of this study by Saint Gobain Research is gratefully acknowledged. The authors gratefully acknowledge the support from the National Science Fund of Bulgaria, Grant no. DO-02-121/2009. The study is under the umbrella of the European project "Beyond Everest" and the COST action MP1106 "Smart and green interfaces".

References

1 J. Binner, in *Cellular Ceramics: Structure, Manufacturing, Properties and Applications*, ed. M. Scheffler and P. Colombo, WILEY-VCH Verlag GmbH & Co. KGaA, 2005, pp. 33–56.
2 P. Colombo, *Philos. Trans. R. Soc., A*, 2006, **364**, 109–124.
3 U. T. Gonzenbach, A. R. Studart, D. Steinlin, E. Tervoort and L. J. Gauckler, *J. Am. Ceram. Soc.*, 2007, **90**, 3407–3414.
4 U. T. Gonzenbach, A. R. Studart, E. Tervoort and L. J. Gauckler, *Angew. Chem., Int. Ed.*, 2006, **45**, 3526–3530.
5 A. Dekoninck, N. Denkov, I. Lesov, S. Tcholakova and K. Golemanov, WIPO Patent, WO 2013/007958 A1, 2013.
6 C. J. Brinker and G. W. Scherer, in *Sol–Gel Science: The Physics and Chemistry of Sol–Gel Processing*, Academic Press, Inc., 1990, pp. 453–509.
7 M. K. Krokida and Z. B. Maroulism, *Drying Technol.*, 1997, **15**, 2441–2458.
8 J. Madiouli, J. Sghaier, D. Lecomte and H. Sammouda, *Food Bioprod. Process.*, 2012, **90**, 43–51.
9 T. K. Sherwood, *Ind. Eng. Chem.*, 1929, **21**, 12–16.
10 T. K. Sherwood, *Ind. Eng. Chem.*, 1929, **21**, 976–980.
11 T. K. Sherwood, *Trans. Am. Inst. Chem. Eng.*, 1931, **27**, 190–202.
12 T. Kawaguchi, J. Iura, N. Taneda, H. Hishikura and Y. Kokubu, *J. Non-Cryst. Solids*, 1986, **82**, 50–56.
13 P. G. Simpkins, D. W. Johnson Jr and D. A. Fleming, *J. Am. Ceram. Soc.*, 1989, **72**, 1816–1821.
14 T. Kawaguchi, H. Hishikura and J. Iura, *J. Non-Cryst. Solids*, 1988, **100**, 220–225.
15 M. E. Katekawa and M. A. Silva, *Drying Technol.*, 2006, **24**, 5–20.
16 S. Khalloufi, C. Almeida-Rivera and P. Bongers, *J. Food Eng.*, 2010, **97**, 177–187.
17 S. J. Kowalski and A. Pawlowski, *Chem. Eng. Sci.*, 2011, **66**, 1893–1905.
18 M. Yamane and T. Kojima, *J. Non-Cryst. Solids*, 1981, **44**, 181–190.
19 W. D. Kingery and J. Francl, *J. Am. Ceram. Soc.*, 1954, **37**, 596–602.
20 G. W. Scherer, *J. Am. Ceram. Soc.*, 1990, **73**, 3–14.
21 M. N. Rad and N. Shokri, *Geophys. Res. Lett.*, 2012, **39**, L04403.
22 G. W. Scherer, *Cem. Concr. Res.*, 2004, **34**, 1613–1624.
23 P. Coussot, *Eur. Phys. J. B*, 2000, **15**, 557–566.
24 S. Whitaker and W. T. H. Chou, *Drying Technol.*, 1983, **1**, 3–33.
25 N. Ceaglske and O. A. Hougen, *Trans. Am. Inst. Chem. Eng.*, 1937, **33**, 283–314.
26 M. Prat, *Drying Technol.*, 1991, **9**, 1181–1208.
27 J. van Brakel and P. M. Heertjes, in *Proc. First Int. Symp. Drying*, Science Press, Princeton, 1978, pp. 70–75.
28 M. Kaviany and M. Mittal, *Int. J. Heat Mass Transfer*, 1987, **30**, 1407–1418.
29 P. Chen and D. C. T. Pei, *Int. J. Heat Mass Transfer*, 1989, **32**, 297–310.
30 A. G. Yiotis, I. N. Tsimpanogiannis, A. K. Stubos and Y. C. Yortsos, *J. Colloid Interface Sci.*, 2006, **297**, 738–748.
31 P. Lehmann, S. Assouline and D. Or, *Phys. Rev. E: Stat. Phys., Plasmas, Fluids, Relat. Interdiscip. Top.*, 2008, **77**, 056309.
32 P. Faure and P. Coussot, *Phys. Rev. E: Stat. Phys., Plasmas, Fluids, Relat. Interdiscip. Top.*, 2010, **82**, 036303.
33 M. Prat, *Chem. Eng. Technol.*, 2011, **34**, 1029–1038.
34 E. Keita, P. Faure, S. Rodts and P. Coussot, *Phys. Rev. E: Stat. Phys., Plasmas, Fluids, Relat. Interdiscip. Top.*, 2013, **87**, 062303.
35 F. K. Juillerat, U. T. Gonzenbach, P. Elser, A. R. Studart and L. J. Gauckler, *J. Am. Ceram. Soc.*, 2011, **94**, 77–83.
36 I. Lesov, S. Tcholakova and N. Denkov, in preparation.
37 S. Guignot, S. Faure, M. Vignes-Adler and O. Pitois, *Chem. Eng. Sci.*, 2010, **65**, 2579–2585.